Laminar Flow and Heat Transfer in a Duct with Contrarotating Wall Sections

L. Burmeister and K. Wong[1]

Velocity and temperature distributions were numerically determined for forced laminar flow of a constant property fluid in a straight circular duct with contrarotating wall sections.

The Reynolds number based on average axial velocity, V_a, was set to 10; the ratio V_W/V_a of wall circumferential velocity, V_W, to V_a was 0, 1, and 10. The axial and circumferential friction coefficients were determined as a function of both distance from the duct inlet and angular position. For large V_W/V_a, regions of reversed flow occur, and the axial friction coefficient averaged over the circumference decreases to a minimum from a high value near the inlet and then rises to asymptotically approach a constant value far downstream where the flow is fully developed. The local circumferential friction coefficient takes on large values at the places where the contrarotating wall sections meet, due to a velocity singularity there. The hydrodynamic entrance length was only slightly increased by the wall velocity for the range of V_W/V_a studied.

The secondary flow induced by the contrarotating walls causes the heat transfer coefficient to vary around the duct periphery, resulting in a substantial increase in the average heat transfer coefficient in the fully-developed region. The thermal entrance length was only slightly increased by the wall velocity for the range of parameters studied.

INTRODUCTION

Swirling fluid flow occurs in such rotating devices as turbines and in curved stationary ducts. Studies of these swirling flows in curved ducts [1,2], cooling systems of rotors [3,4], some industrial heat exchangers [5] and some manufacturing processes [6] are available.

When a nonrotating fluid enters a straight duct rotating about its centerline, a secondary flow in the plane perpendicular to the main flow is created that can alter the axial velocity pattern from that found in a stationary duct. Following an early experimental study by Levy [7] of the effect of pipe rotation on hydraulic loss, later followed by the measurements of Shchukin [8], Nuttal [9] investigated swirling fluid flow in a stationary vertical pipe at high axial Reynolds numbers and reported for the first time that reverse flow occurs in the center of the pipe for some swirl rates and axial flow rates. The flow reversal associated with rotating ducts drew the attention of Talbot [10], who used a perturbation method to obtain an analytical solution for the decay of swirl velocity in a stationary pipe. Binnie [11] studied a weak swirling flow at low Reynolds number in a horizontal stationary pipe and reported a different reversed flow pattern. Inspired by the works of Binnie and Talbot, Deka [12]

1. Dept. of Mechanical Engineering, University of Kansas, Lawrence, KS, USA 66049-2234.

Scientia Iranica, Vol. 1, No. 2, © Sharif University of Technology, July 1994.

studied the motion of swirling viscous liquid through an infinitely long stationary circular pipe. Assuming the swirl to be small, Deka solved the perturbed Navier-Stokes equations for the swirl and axial velocities. His solutions show that the swirling flow could cause the fluid at the centerline to reverse its direction. Profiles of flow velocity in a rotating pipe were analytically obtained by Lavan et al. [13], following White's [14] examination of the characteristics of fully-developed flow in rotating pipes. Their studies encompassed two types of phenomena: the decay of the swirl occurring when a swirling flow enters a stationary duct, and the generation of swirl in a nonrotating flow that enters a rotating duct. They reported that when a rotating fluid enters a stationary duct, a region of low axial velocity near the center, or even a region of reversed flow, tends to form on the axis. The shear at the wall is larger than in a flow without rotation. When a nonswirling fluid enters a rotating tube, a region of separated flow tends to form on the tube wall, resulting in smaller wall shear stress than that found in straight flow.

Cannon and Kays [15] experimentally studied heat transfer to a fluid flowing inside a pipe rotating about its centerline. They found that the rotation tends to increase the Reynolds number for transition from laminar to turbulent flow, and the most pronounced effect of rotation on heat transfer occurs with laminar flow. Later studies by others [16–24] concentrated on turbulent flow, although Reich and Beer [24] discuss the effect of wall velocity on laminar-to-turbulent transition.

Recently, cases in which various portions of the duct wall are in contramotion have been studied as well. Chen et al. [25] numerically solved the problem of a square cavity with moving walls; included was the case in which top and bottom walls both move at the same speed from left to right with the two vertical walls stationary. These driven-cavity problems had no flow along the axis of the duct. More recently Litsek and Bejan [26] and Litsek et al. [27] studied a similar driven-cavity problem, that of convection in the cavity formed between two cylindrical rollers, a moving load and a moving support. Chen, Litsek and Bejan, and Litsek et al. found regions of recirculating flow; the latter two also found the heat transfer coefficients between the moving convex roller surface and the enclosed fluid.

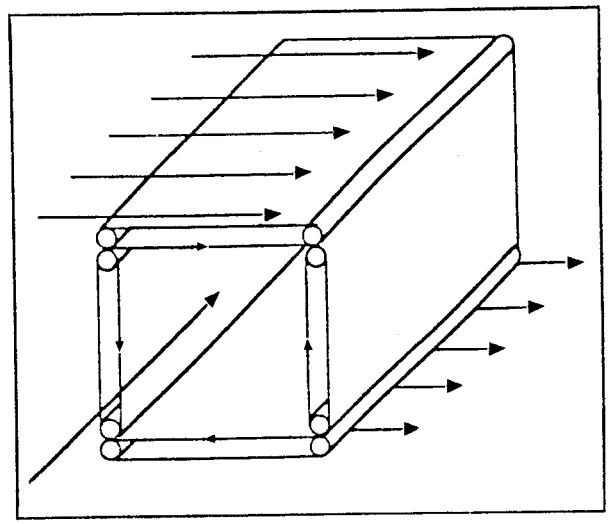

Figure 1. A contrarotating-wall heat exchanger of rectangular cross section.

It seems that utilization of the swirling flow, generated by means of contrarotating heat transfer surfaces about the centerline of a duct to improve its performance as a heat exchanger, has not previously been investigated. The objective of the present study is to numerically simulate the flow and heat transfer in a contrarotating-wall duct to provide a basis for assessing its merit for improving heat exchanger performance.

A physically-realizable contrarotating-wall duct is shown in Figure 1. Eight rollers, each pair occupying a corner of the duct, support and drive four belts. One fluid flows down the duct and another fluid passes transversely across the duct.

PROBLEM FORMULATION

A potential advantage of a contrarotating-wall heat exchanger over a conventional heat exchanger is the use of the secondary flow generated by the moving walls to enhance the

heat transfer process at the wall. A measure of control of the heat transfer rate would be possible since the rate of energy transfer can be varied by changing the rotational speed of the walls. The secondary flow mixes the fluid near the wall, where the heat transfer process takes place, with the fluid in the core. This mixing process distributes the transferred energy throughout the flow field.

In this section, the procedure is set forth by which effects of the moving walls on the secondary flow and the nature of the mixing process were investigated by studying a driven cavity flow similar to that encountered in a contrarotating-wall heat exchanger. In the simplified case selected for analysis, the walls of the duct contrarotate about the centerline of the duct as shown in Figure 2; leakage at the junction of the moving walls that can be encountered in rotating regenerative heat exchangers is neglected.

In each quadrant, the wall of the circular duct moves in the direction indicated in Figure 2. With this geometry, the lines of symmetry for the driven cavity flow are along the radial coordinate direction lines in cylindrical coordinates. Thereby, the number of solution points needed to achieve accuracy in a numerical method is reduced by a factor of four.

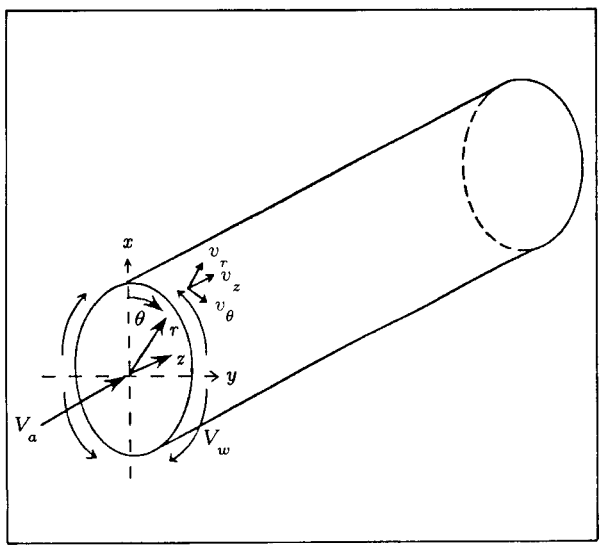

Figure 2. Flow in a duct with contrarotating-wall sections.

For a Newtonian fluid with constant properties, the equations of motion, [28] are:

r Component

$$\varrho\left(v_r\frac{\partial v_r}{\partial r}+\frac{v_\theta}{r}\frac{\partial v_r}{\partial_\theta}-\frac{v_\theta^2}{r}+v_z\frac{\partial v_r}{\partial z}\right)$$
$$=-\frac{\partial p}{\partial r}+\mu\left[\frac{\partial}{\partial r}\left(\frac{1}{r}\frac{\partial}{\partial r}(rv_r)\right)\right.$$
$$\left.+\frac{1}{r^2}\frac{\partial^2 v_r}{\partial\theta^2}-\frac{2}{r^2}\frac{\partial v_\theta}{\partial\theta}+\frac{\partial^2 v_r}{\partial z^2}\right],$$
$$0\le r<R$$
$$0\le\theta<360^\circ \qquad (1)$$
$$0\le z,$$

θ Component

$$\varrho\left(v_r\frac{\partial v_\theta}{\partial r}+\frac{v_\theta}{r}\frac{\partial v_\theta}{\partial\theta}+\frac{v_r v_\theta}{r}+v_z\frac{\partial v_\theta}{\partial z^2}\right)$$
$$=-\frac{1}{r}\frac{\partial p}{\partial\theta}+\mu\left[\frac{\partial}{\partial r}\left(\frac{1}{r}\frac{\partial}{\partial r}(rv_\theta)\right)\right.$$
$$\left.+\frac{1}{r^2}\frac{\partial^2 v_\theta}{\partial\theta^2}+\frac{2}{r^2}\frac{\partial v_r}{\partial\theta}+\frac{\partial^2 v_\theta}{\partial z^2}\right], \qquad (2)$$

z Component

$$\varrho\left(v_r\frac{\partial v_z}{\partial r}+\frac{v_\theta}{r}\frac{\partial v_z}{\partial\theta}+v_z\frac{\partial v_z}{\partial z}\right)=-\frac{\partial p}{\partial z}$$
$$+\mu\left[\frac{1}{r}\frac{\partial}{\partial r}\left(r\frac{\partial v_z}{\partial r}\right)+\frac{1}{r^2}\frac{\partial^2 v_z}{\partial\theta^2}+\frac{\partial^2 v_z}{\partial z^2}\right], \qquad (3)$$

subject to the inlet conditions

$$v_r(r,\theta,0)=0$$
$$v_\theta(r,\theta,0)=0$$
$$v_z(r,\theta,0)=V_a,$$

the wall conditions

$$v_r(R,\theta,z)=0$$
$$v_\theta(R,\theta,z)=V_W$$
$$v_z(R,\theta,0)=0,$$

and the outlet condition that all gradients normal to the exit plane are zero.

The energy equation is

$$\varrho C_p \left(v_r \frac{\partial T}{\partial r} + \frac{v_\theta}{r} \frac{\partial T}{\partial \theta} + v_z \frac{\partial T}{\partial z} \right) = k \left[\frac{1}{r} \frac{\partial}{\partial r} \left(r \frac{\partial T}{\partial r} \right) + \frac{1}{r^2} \frac{\partial^2 T}{\partial \theta^2} + \frac{\partial^2 T}{\partial z^2} \right], \quad (4)$$

subject to the boundary conditions

$$T(R, \theta, z) = T_W$$
$$T(r, \theta, 0) = T_o.$$

The constant-property fluid assumed in this study was air at 293 K with density and viscosity being 1.204 kg/m^3 and 1.81 $\times$ 10^{-5}N s/m^2, respectively. The radius, R, of the duct was 0.1 m, the length was 0.2 m to ensure achievement of fully developed conditions at the outlet and the average forced axial velocity, V_a, gave a Reynolds number, Re, that ranged from 10 to 100. In the second test case, discussed below, V_a was set to zero while V_W was not.

The velocity and temperature distributions of the flow down the duct were numerically determined by use of FLUENT, an interactive menu-driven computer code for solving the Navier-Stokes and energy equations based on a finite volume method [29–31]. The numerical results obtained by FLUENT were plotted by use of PLOT 3D, a numerical flow-visualization code developed at NASA [32]. A FORTRAN computer code was developed to compute friction coefficients, Nusselt numbers and various other quantities from the velocities and temperatures obtained with FLUENT.

TEST CASES

To assist in establishing the number and size of the mesh employed in the numerical flow simulation, a case of known solution was first solved. This case was the two-dimensional one of air entering a duct of stationary walls ($V_W = 0$) at a uniform velocity ($V_a = 7.5166 \times 10^{-3}$ m/s). The fully-developed axial friction coefficient $C_f = 2\tau_w/\varrho V_a^2$ was found to be given by $C_f Re = 16.125$, only 0.78% higher than the exact value of $C_f Re = 16$. This result did not change after two doublings of the number of both radial and axial grid points. The entrance loss coefficient K in the expression for pressure loss

$$(p_o - p)/(\varrho V_a^2/2) = \frac{64}{Re} \frac{z}{D} + K, \quad (5)$$

was found to be 1.07, compared to the experimental value of 1.24 cited by White [33] as being most realistic. The Nusselt number for fully developed conditions was similarly found to be about 1% above the exact value of 3.658.

A second test case was the two-dimensional one of the contrarotating wall-driven cavity flow that is the present problem without axial flow ($V_a = 0$). The solution to this problem was not known to the authors. Four different mesh sizes were used; the number of nodes used in each of the radial and circumferential directions was doubled in each subsequent refinement. One hundred forty-four equally spaced nodes were used first, 12 in each of the radial and circumferential directions. Twenty-two nodes in both the radial and circumferential directions, for a total of 448 nodes, were used second. Forty-two nodes in both the radial and circumferential directions were used third. Eighty-two nodes in each of the radial and circumferential directions were used fourth. The number of nodes needed to achieve a grid-independent solution was reduced by a factor of four by taking advantage of the symmetry of this problem to obtain numerical solutions in only one quadrant, $0° \leq \theta \leq 90°$. The planes of symmetry at $\theta = 0°$ and 90° were with zero normal gradients and zero normal flow.

A vector plot of the computed velocity in the second test case is given in Figure 3. As shown in this figure, the shear stress at the anti-clockwise-moving wall causes the fluid particles to swirl anti-clockwise. Also, a fluid particle adjacent to the moving wall at either end of the wall is abruptly forced to change its direction. At the 0° line, a particle traveling in the circumferential direction is suddenly forced to move in a vertical radial line without circumferential velocity. At the 90° line, the flow pattern is reversed; the fluid particle moves in

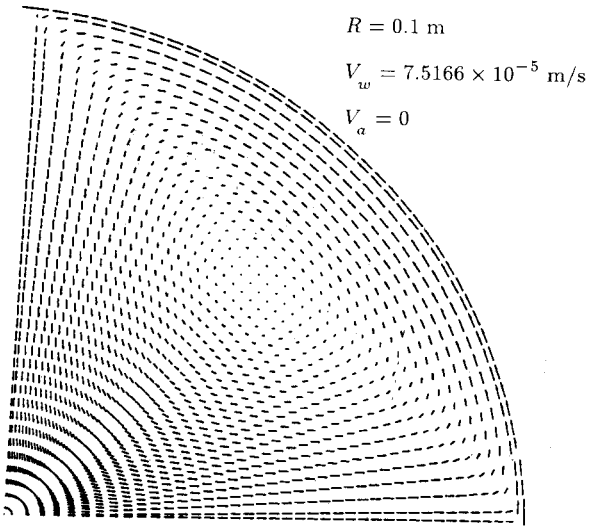

Figure 3. A vector plot of the computed velocity distributions.

a horizontal radial line with no circumferential velocity until it reaches the moving wall, where it is forced to move in the circumferential direction with the wall velocity. This singularity in the circumferential velocity results in the local circumferential friction coefficient being unbounded at both ends of the moving wall.

The circumferential velocity v_θ was normalized by dividing the circumferential velocity by the wall velocity $V_w = 7.5166 \times 10^{-5}$m/s, low enough for creeping flow to ensue. The second test case is plotted against the normalized radial distance at 45° in Figure 4. As shown, the velocities computed with four different mesh sizes are in good agreement. The agreement in the velocity near the wall used to compute the circumferential friction coefficient is excellent. The local circumferential friction coefficient defined as $C_{f\theta} = \tau_{r\theta}/(\varrho V_a^2/2)$ was computed from the velocity distributions obtained for each mesh size. Plots of the circumferential shear stress coefficient versus the circumferential angle for four mesh sizes are in Figure 5. The circumferential stress coefficients in the middle section of the wall for each mesh size agree. The discrepancies at $\theta = 0°$ and 90° are primarily due to the differences in the ability of the mesh sizes to capture the singularities. As more and more nodes were used, the accuracy of the

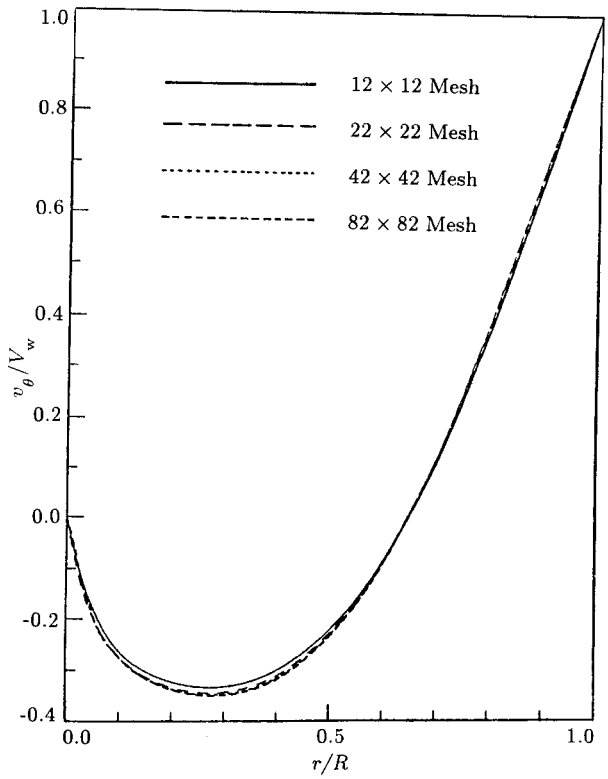

Figure 4. Normalized circumferential velocity versus normalized radial distance, at 45 degrees.

computed velocity distribution was improved, and the singularities of the problem became more evident. In reality, the flow would not have this singularity imposed. The solution presented above is correct in the mathematical sense of the problem posed; the mathematical description is incomplete near the singular points.

NUMERICAL RESULTS FOR TWO CASES

For the original problem posed, both axial and wall velocities are nonzero. In this section, the investigation results with ratios of wall to axial velocities of 1 and 10 are presented for $Re = 10$. Because the wall is not stationary, three-dimensional models were used.

$V_w/V_a = 1$

For $V_w/V_a = 1$, a secondary flow in the plane perpendicular to the main flow is induced by the moving wall. The development of the

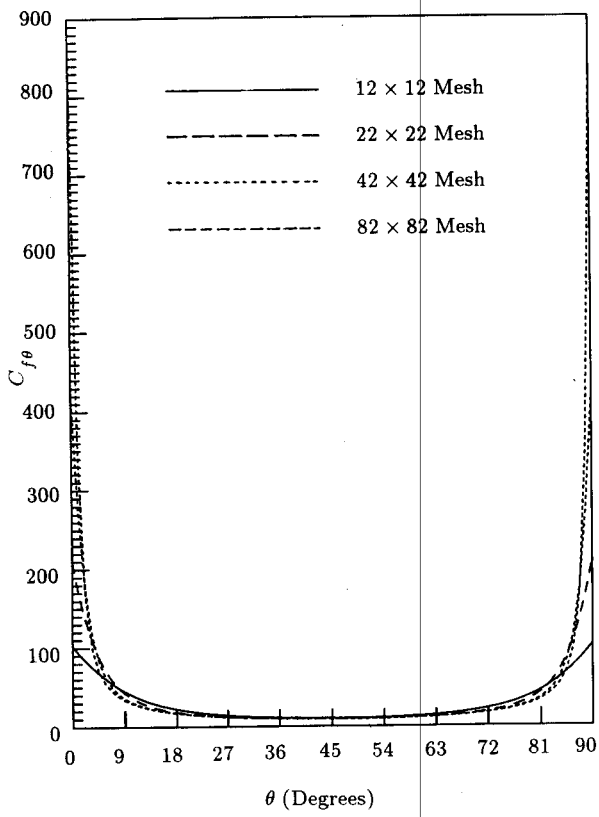

Figure 5. Local circumferential friction coefficient versus angular position.

secondary flow is shown in Figures 6 and 7. The discontinuity in circumferential velocity on the wall at $\theta = 0°$ and 90° is revealed in these figures. Even in the inlet section, Figure 6, the flow pattern has a secondary component, although it is strong only in a thin region near the wall. However, farther from the inlet, the swirling pattern discerned for $V_w = 0$ is established throughout the duct cross section as shown in Figure 7. The axial velocity profiles in the fully-developed region at $\theta = 0°$, 45° and 90° are presented in Figure 8. As shown in this figure, the axial velocity distribution is little affected by the moving wall and remains nearly parabolic in the fully-developed region; the variation of the velocity distribution with θ is also shown. The peak velocity is shifted from the centerline location it occupied at $V_w = 0$ to $r/R = 0.2$ but the basic character of the flow is unchanged from that for the stationary-wall case.

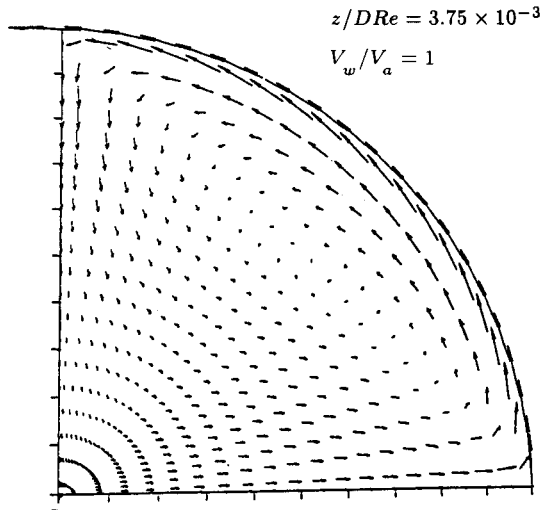

Figure 6. Secondary flow at the entrance region of a contrarotating-wall duct.

The local axial friction coefficient C_f is two dimensional, varying in both the axial and angular directions. To facilitate comparison and interpretation of the results, a circumferentially-averaged axial friction coefficient $\overline{C}_f$ based on V_a was computed by averaging the local value over the circumference and is shown in Figure 9. Although there are discrepancies between these two curves near the inlet, the agreement is good downstream.

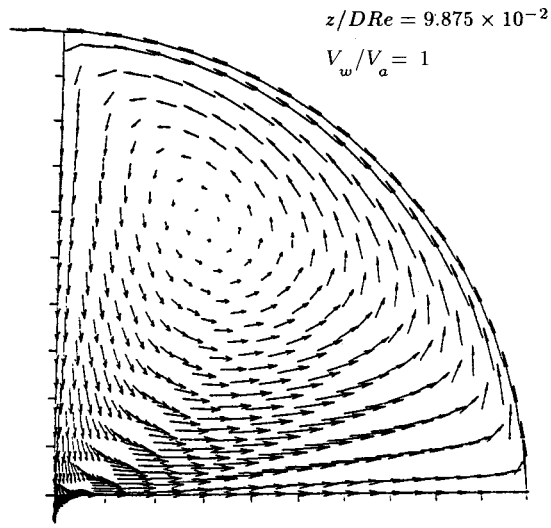

Figure 7. Secondary flow in the exit region of a contrarotating wall duct.

The limiting axial circumferentially-averaged friction coefficient from the finest mesh is 1.748 as compared to 1.641 computed for $V_w = 0$ (the exact friction coefficient for $V_w = 0$ is 1.6); this represents an increase of 6.5% in friction coefficient.

Rotation of the heat transfer surface creates an additional shear stress $\tau_{r\theta}$ in the circumferential direction. The circumferential friction coefficient $C_{f\theta}$ based on V_a at various axial locations is presented in Figure 10. The coefficient is symmetric about the $\theta = 45°$ plane and the variation with θ is small except for the regions near the edges of the surface where it becomes large at $\theta = 0°$ and $\theta = 90°$. The circumferential shear stress becomes large at these locations since a circumferential velocity discontinuity exists at the wall on these planes, and the gradient of the circumferential velocity is infinite there, as discussed before. Although an average circumferential friction coefficient

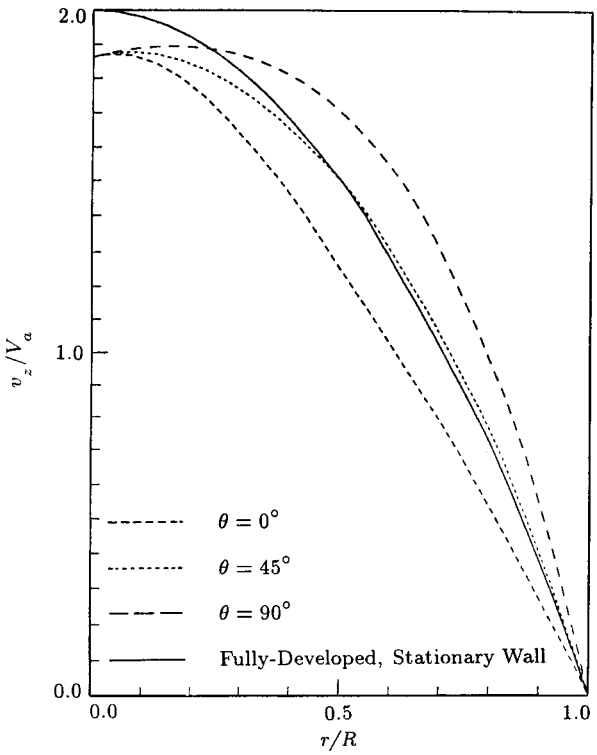

Figure 8. Normalized axial velocity profiles in the full-developed region of a contrarotating-wall duct $V_w/V_a = 1$.

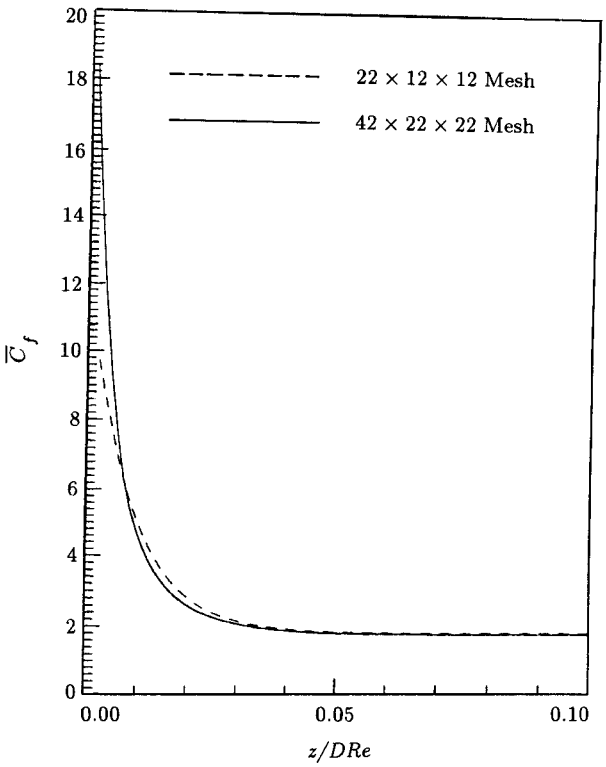

Figure 9. Local axial friction coefficient in the entrance region of a contrarotating-wall duct at selected axial locations: $V_w/V_a = 1$.

over the entire surface cannot be evaluated due to the singularity on the edges, an average value $\overline{C}_{f\theta}$ can be obtained by averaging the coefficient from $\theta = 9°$ and $\theta = 81°$. This average value can be used to estimate the power required to move the wall. The circumferential friction coefficient averaged from $\theta = 9°$ to $\theta = 81°$ is given in Figure 11 where the limiting value is seen to be 1.565.

The Nusselt number was computed from the temperature and velocity distributions obtained by use of FLUENT. The circumferentially-averaged value $\overline{Nu}$ was computed from the local Nusselt number and is shown in Figure 12. The solid line is the result from the finer mesh; the dashed line is the result from the coarser mesh. The behaviors of these curves are similar to those found with $V_w = 0$; the Nusselt number is larger near the inlet and gradually approaches a limiting value of 4.121. The limiting Nusselt number for $V_w = 0$ is 3.849 as computed (3.658 is the

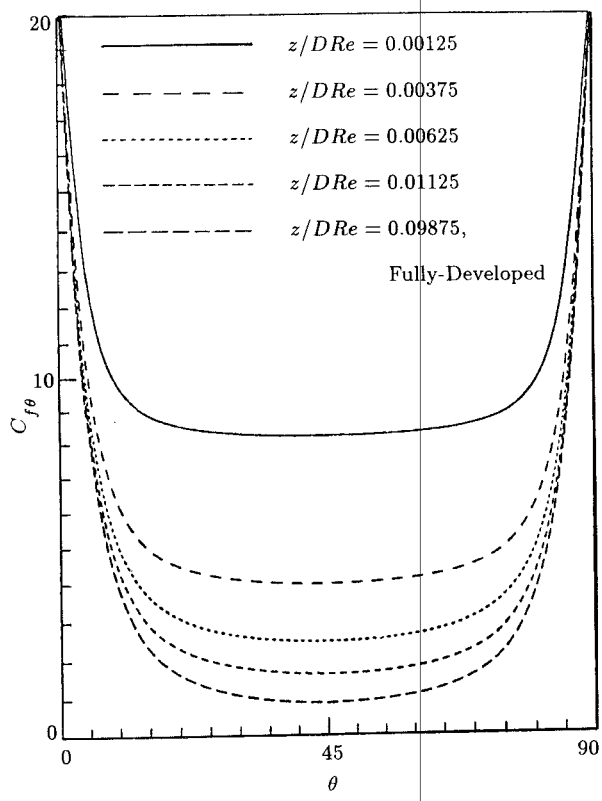

Figure 10. Local, circumferentially-averaged axial friction coefficient in the entrance region of a contrarotating-wall duct: $V_w/V_a = 1$.

exact value). Therefore, a 7.1% higher limiting Nusselt number is obtained by rotating the heat transfer surface at $V_w/V_a = 1$.

$V_W/V_a = 10$

For $V_W/V_a = 10$, the flow induced by the moving wall is strong compared to the axial flow. While many characteristics are as previously discussed for lower values of the V_W/V_a ratio, especially in the entrance region, new features arise.

The three-dimensional plot of axial velocity versus position in the duct in Figure 13 shows that regions of separated flow occur near the wall and regions of reversed flow occur in the center. Of course, the axial velocity is higher than for a stationary wall in the other regions. Such reversed flow, although unusual, has been observed by others in flows involving a change in fluid swirl induced by either a rotating duct wall or a curved duct.

The circumferentially-average circumferential shear stress coefficient $\overline{C}_{f\theta}$, shown in Figure 14, displays the trends seen at lower values of the V_W/V_a parameter, but new behaviors are observed for the circumferentially-averaged axial friction coefficient $\overline{C}_f$ and Nusselt number $\overline{Nu}$ as shown in Figures 15 and 16, respectively. There it is seen that both quantities initially diminish from large values at the inlet to a local minimum in the entrance region before rising to asymptotically approach a higher limit in the fully-developed flow region at the outlet. The length L_e of the hydrodynamic entrance region is seen in Figure 15 to have increased by a factor of about 2 above the value given by the conventional criterion $L_e/DRe \approx 0.05$. This observation applies as well to the thermal entrance region as illustrated in Figure 16.

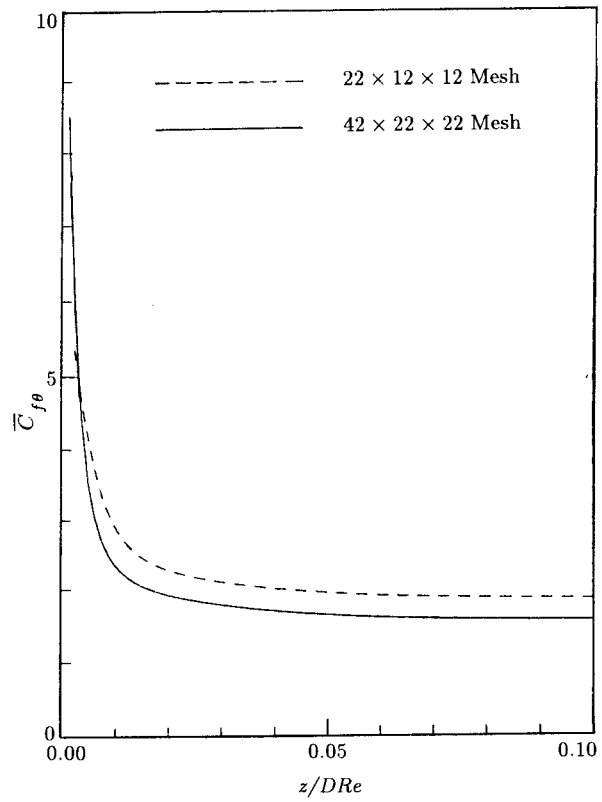

Figure 11. Local, circumferentially-averaged circumferential friction coefficient in the entrance region of a contrarotating-wall duct at selected axial locations: $V_w/V_a = 1$.

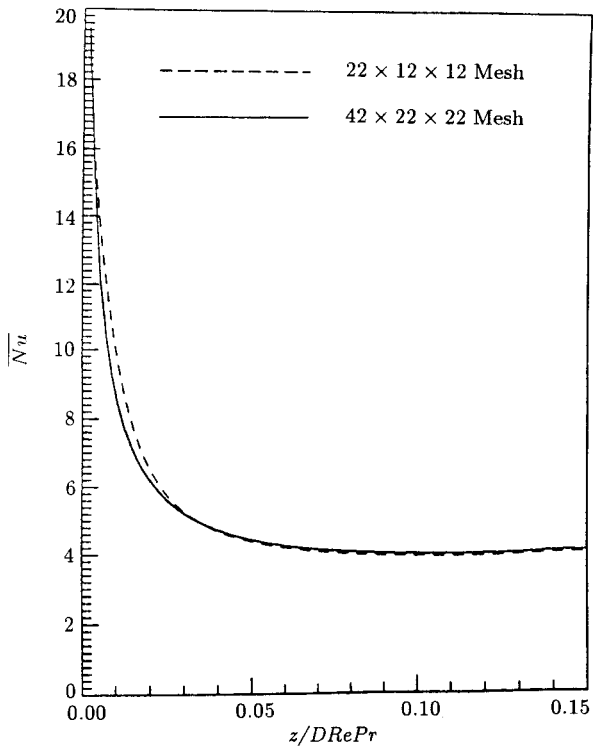

Figure 12. Local, circumferentially-averaged Nusselt number in the entrance region of a contrarotating-wall duct with a constant wall temperature of 393 K: $V_w/V_a = 1$.

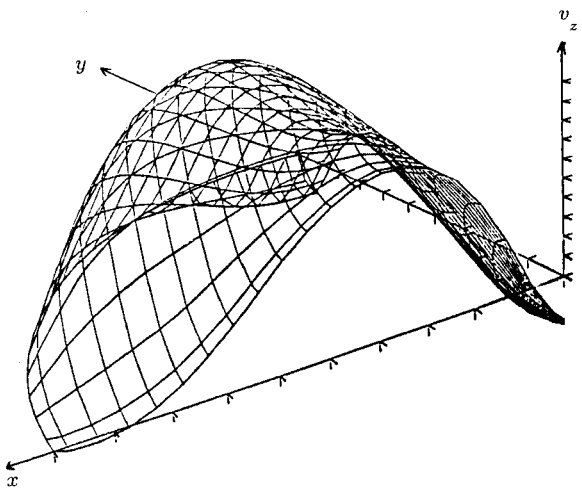

Figure 13. Axial velocity at a downstream position with flow reversal in the duct center and with flow separation at the wall ($60° < \theta < 90°$): $V_w/V_a = 10$.

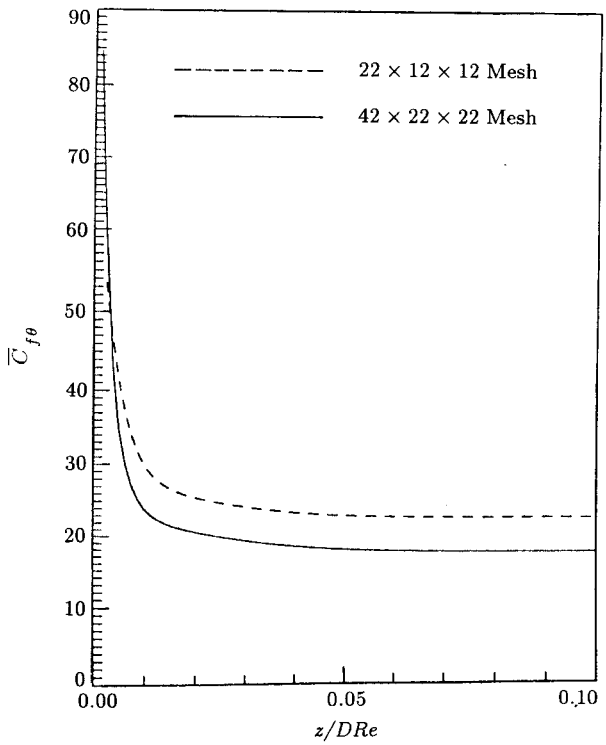

Figure 14. Local, circumferentially-averaged circumferential friction coefficient in the entrance region of a contrarotating-wall duct: $V_w/V_a = 10$.

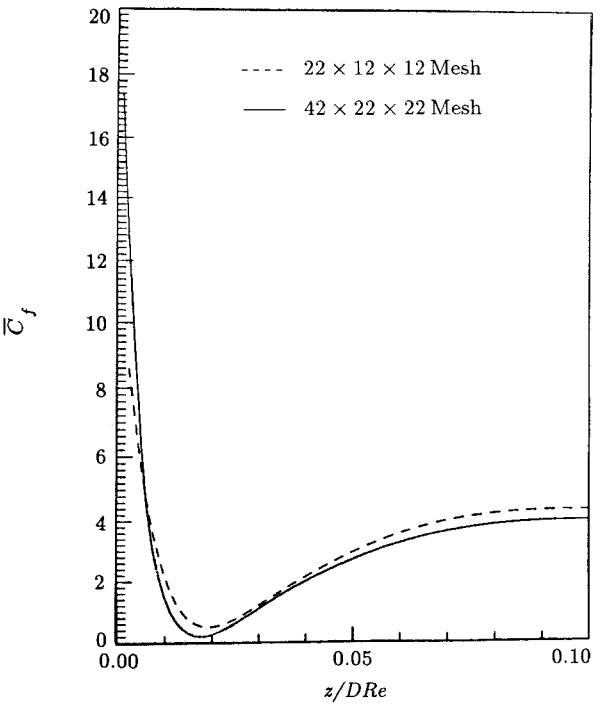

Figure 15. Local, circumferentially-averaged axial friction coefficient in the entrance region of a contrarotating-wall duct: $V_w/V_a = 10$.

GENERAL RESULTS

The circumferentially-averaged axial friction coefficients obtained for seven velocity ratios V_W/V_a are plotted in Figure 17. As seen there, the axial friction coefficient is little affected by V_W/V_a and monotonically approaches a limiting value at the duct outlet where the flow is fully developed. However, for V_W/V_a greater than six, the axial friction coefficient decreases to a minimum before asymptotically approaching a higher constant value downstream. The local minimum is due to the flow reversal near the wall that occurs in the early stage of the velocity development. The intensity of the flow reversal increases with the increase in the wall velocity, causing the minimum to decrease as the velocity ratio increases at a location that moves toward the inlet as the velocity ratio increases. After the flow reversal, the fluid reattaches onto the wall, as evidenced by the asymptotic increase of the local axial

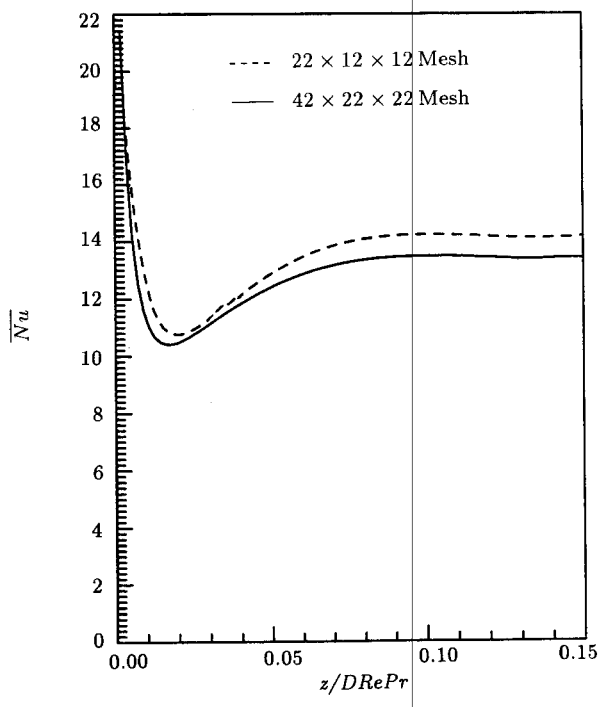

Figure 16. Local, circumferentially-averaged Nusselt number in the entrance region of a contrarotating-wall duct with a constant wall temperature of 393 K: $V_w/V_a = 10$.

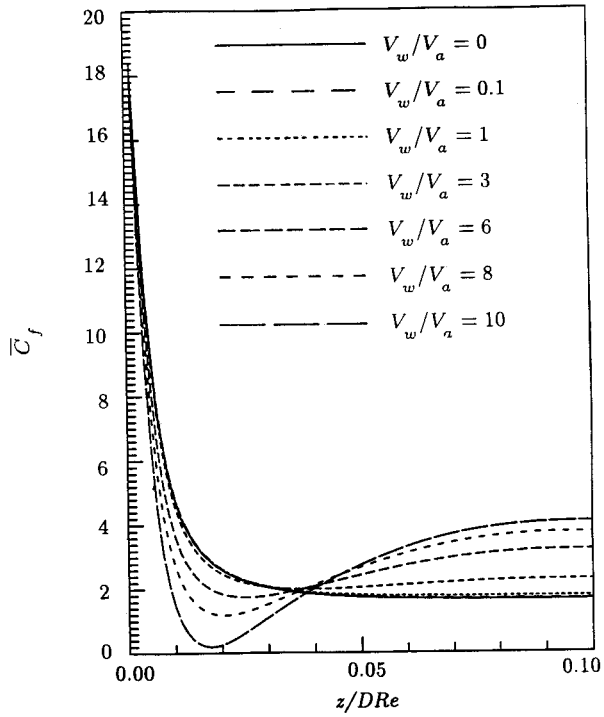

Figure 17. Local, circumferentially-averaged axial friction coefficient, C_f, in the entrance region.

friction coefficient from the minimum. The circumferentially-averaged axial friction coefficient $\overline{C}_{f2}$, based on the velocity magnitude $(V_W^2 + V_a^2)^{1/2}$ versus the dimensionless axial distance z/DRe, is shown in Figure 18 to follow the trends observed for the axial friction coefficient based on the axial velocity with the exception that $\overline{C}_{f2}$ decreases with increasing velocity ratio. The limiting axial friction coefficients, normalized by the limiting value $C_{f,0} = 1.641$ for a stationary duct, are shown in Figure 18 as function of the velocity ratio for which correlations are

$$\frac{\bar{C}_{f,\infty}}{C_{f,0}} = \begin{cases} 1, & V_W/V_a \leq 1.6, \\ 0.789(V_W/V_a)^{0.508}, & V_W/V_a \geq 1.6, \end{cases} \tag{6}$$

and

$$\frac{\bar{C}_{f2,\infty}}{C_{f,0}} = \begin{cases} 1, & V_W/V_a \leq 0.65 \\ 0.559(V_W/V_a)^{-1.337}, & V_W/V_a \geq 0.65. \end{cases} \tag{7}$$

It can be seen that the axial friction coefficient based on the axial velocity is unaffected by velocity ratios below 1.6, but increases as the 0.508 power of the velocity ratio for values above 1.6. The axial friction coefficient based on the velocity magnitude is unaffected by velocity ratios below 0.65, but decreases as the -1.337 power of the velocity ratio for values above 0.65.

The circumferentially-averaged circumferential friction coefficient $\overline{C}_{f\theta}$, based on the axial velocity, is displayed versus dimensionless distance from the inlet in Figure 19. It is seen that $\overline{C}_{f\theta}$ has a large value at the inlet and monotonically approaches a limiting value at the outlet, a value that increases as the velocity ratio increases with a correlation of

$$\frac{\overline{C}_{f\theta,\infty}}{C_{f,0}} = 0.943(V_W/V_a)^{1.003}. \qquad (8)$$

The corresponding circumferential friction coefficient based on the velocity magnitude is shown in Figure 20 to increase with increasing

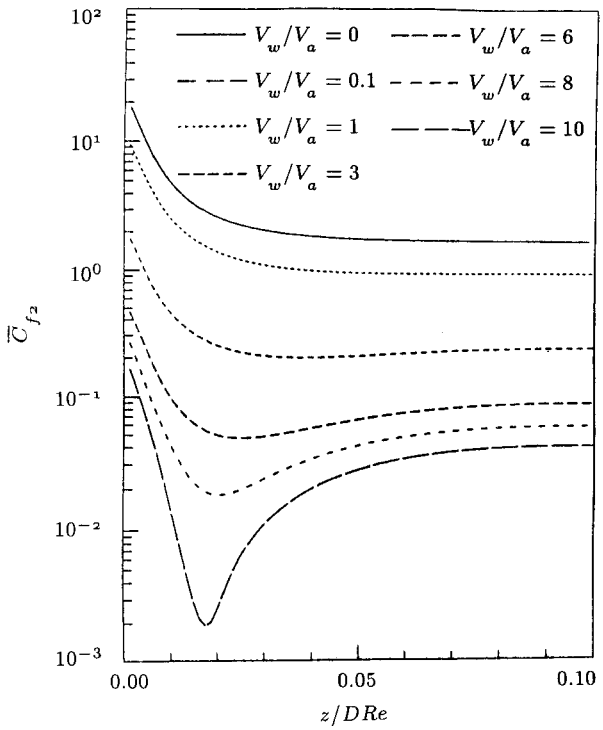

Figure 18. Local, circumferentially-averaged friction coefficient, C_{f2}, based on the velocity magnitude.

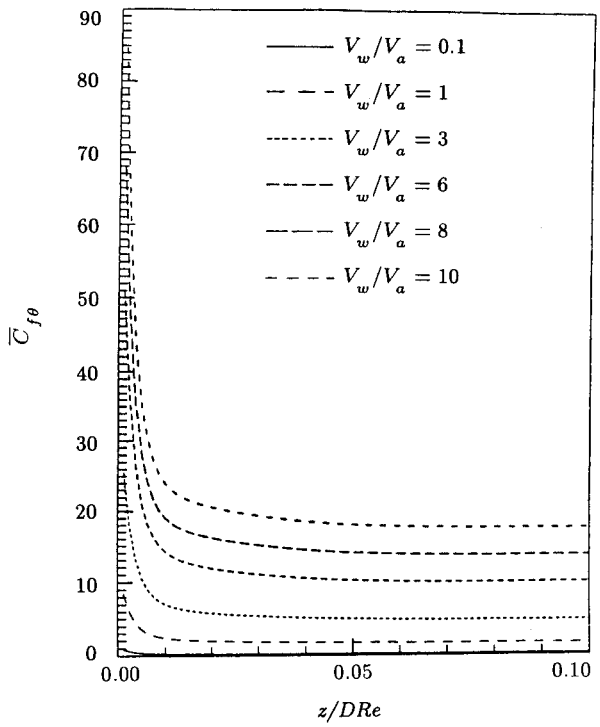

Figure 19. Local, circumferentially-averaged circumferential friction coefficient, $C_{f\theta}$, in the entrance region.

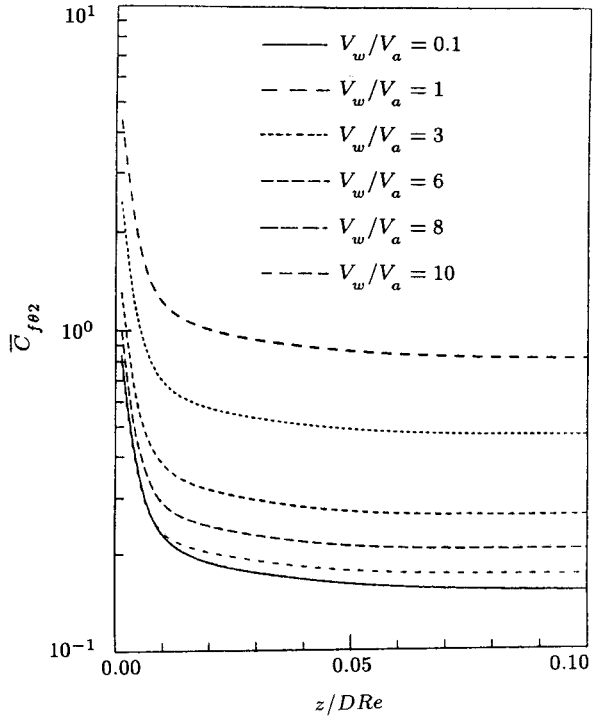

Figure 20. Local, circumferentially-averaged circumferential friction coefficient, $C_{f\theta 2}$, based on the velocity magnitude in the entrance region.

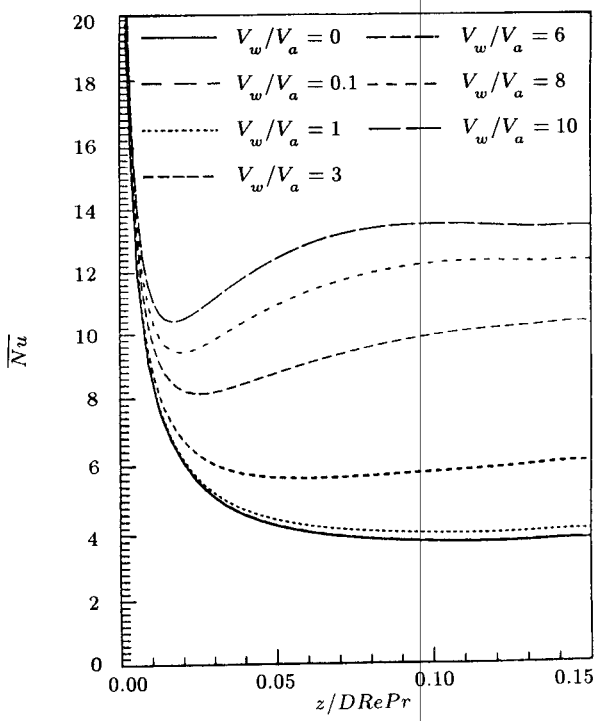

Figure 21. Local, circumferentially-averaged Nusselt number in the entrance region.

velocity ratio until the velocity ratio exceeds a value of 1.26, after which the friction coefficient decreases with increasing velocity ratio as

$$\frac{\overline{C}_{f2,\infty}}{C_{f,0}} = \begin{cases} 0.499(V_W/V_a)^{0.731}, & V_W/V_a \leq 1.26 \\ 0.720(V_W/V_a)^{-0.837}, & V_W/V_a \geq 1.26. \end{cases} \tag{9}$$

The circumferentially-averaged Nusselt numbers are displayed in Figure 21. As seen there, when the velocity ratio is less than three, the Nusselt number monotonically decreases from a large value at the inlet to a limiting value at the outlet where flow is fully developed. Only slight increases of the limiting value occur with increasing velocity ratio in this range. At velocity ratios of six or higher, the Nusselt number decreases to a minimum near the inlet and rises to asymptotically approach a limiting value. As for the axial friction coefficient, the limiting value increases, the minimum value decreases and the location of the minimum moves toward the inlet with increasing velocity ratio. These results are correlated after normalizing by the limiting value $Nu_0 = 3.849$ for a stationary duct by

$$\frac{\overline{N}_{u,\infty}}{Nu_0} = \begin{cases} 1, & V_W/V_a \leq 1.6 \\ 0.710(V_W/V_a)^{0.724}, & V_W/V_a \geq 1.6. \end{cases} \tag{10}$$

The Nusselt number varies as the 0.724 power of the velocity ratio, whereas the circumferentially-averaged axial friction coefficient varies as the 0.508 power, both for velocity ratios exceeding a value of 1.6. While the circumferentially-averaged circumferential friction coefficient varies as the 1.003 power of the velocity ratio, a more rapid variation than for the Nusselt number, the power P required to pump the fluid through the duct and to maintain the duct wall rotation is given by

$$P = \left(\overline{C}_f 2\pi RL + \overline{C}_\theta 2\pi R^2 L\right) V_a^2/2, \tag{11}$$

and is seen primarily to be affected by the axial friction factor, the first term in parentheses, for ducts of small radius. Hence, an increase in velocity ratio will increase the heat transfer rate from the wall to the fluid, through its relationship with the Nusselt number, more than pumping-wall rotation power for such ducts.

Finally, the entrance lengths were extracted from the velocity and temperature distributions. The entrance length L_e was taken to be the location at which the local circumferentially-averaged axial friction coefficient departs from the asymptotic value by only 1%. Similarly, $L_{e\theta}$ and L_{eT} are the circumferentially-averaged circumferential friction coefficient entrance length and the thermal entrance length, respectively. All three are given in Table 1, where it is seen that they are only slightly dependent upon the velocity ratio in the range studied.

Additional details of method and result are given by Wong [34], as stated earlier [35].

CONCLUSIONS

The major effects of contrarotating walls on forced laminar flow in a circular duct have been

Table 1. Dimensionless entrance lengths for a cylindrical duct with contrarotating wall sections.

V_w/V_a	$\frac{L_e}{(x/DRe)}$	$\frac{L_{e\theta}}{(x/DRe)}$	$\frac{L_{eT}}{(x/DRe)}$
0.1	0.067	0.074	0.075
1	0.071	0.073	0.069
3	0.081	0.054	0.132
8	0.056	0.056	0.097
10	0.088	0.057	0.077

numerically determined. The increase in axial friction coefficient is accompanied by a large increase in heat transfer coefficient and by a circumferential friction coefficient.

Under some conditions, the interactions of a large wall velocity and forced axial flow lead to regions of reversed flow. Local minima of circumferentially-averaged heat transfer coefficient and axial friction coefficient are then observed in the entrance region.

ACKNOWLEDGEMENT

The numerical computations were performed on the VAX 9000, Model 210 computer in the Computation Center of the University of Kansas.

NOMENCLATURE

English Symbols

C_f local axial friction coefficient, $\tau_{rz}/(V_a^2/2)$

$C_{f\theta}$ local circumferential friction coefficient, $\tau_{r\theta}/(V_a^2/2)$

C_p fluid specific heat at constant pressure, kJ/kg K

D duct diameter, m

h convective heat transfer coefficient, W/m^2K

k fluid thermal conductivity , $W/m\ K$

L_e hydrodynamic entrance length, m

L_{eT} thermal entrance length, m

Nu local Nusselt number, hD/k

p pressure

p_o inlet pressure

P power

Pr Prandtl number, $\mu\ C_p/k$

q heat transfer rate, W

r radial coordinate, m

R duct radius, m

Re Reynolds number based on average velocity, $\varrho V_a D/\mu$

T temperature, K

T_m mixing-cup temperature, K

T_o inlet temperature, K

T_W wall temperature, K

v_r radial velocity, m/s

v_z axial velocity, m/s

v_θ circumferential velocity, m/s

V_a average axial inlet velocity, m/s

V_W wall velocity, m/s

z axial distance from the inlet, m

Greek Symbols

μ fluid viscosity, N s/m^2

θ angular coordinate, degree

ϱ fluid density, kg/m^3

$\tau_{r\theta}$ circumferential wall shear stress, N/m^2

τ_{rz} axial wall shear stress N/m^2

Superscripts

$-$ circumferentially averaged

Subscripts

2 based on $v_a^2 + v_w^2, \bar{\tau}_{rz}/\left[(v_a^2 + v_w^2)/2\right] = \overline{C}_{f2}$

REFERENCES

1. Yee, G., Chilukuri, R. and Humphrey, J.A.C. "Developing flow and heat transfer in strongly curved ducts of rectangular cross section", *ASME J. Heat Transfer*, **102**, pp 285–291 (1980).

2. Hwang, G.J. and Chao, C.-H. "Forced laminar convection in a curved isothermal square duct", *ASME J. Heat Transfer*, **113**, pp 48–55 (1991).

3. Metzger, D.E. and Afghan, N.H. *Heat and Mass Transfer in Rotating Machinery*, Hemisphere, New York (1984).

4. Morris, W.D. *Heat Transfer and Fluid Flow in Rotating Coolant Channels*, Research Studies Press (Div. of Wiley & Sons), New York (1981).

5. Mori, Y. and Nakayama, W. "Study of forced convective heat transfer in curved pipes", *Int. J. Heat Mass Transfer*, **10**, pp 37–59 and 681–695 (1967).

6. Lin, Y.T., Choi, M. and Greif, R. "A three-dimensional analysis of the flow and heat transfer for the modified chemical vapor deposition process including buoyancy, variable properties and tube rotation", *ASME J. Heat Transfer*, **113**, pp 400–406 (1991).

7. Levy, F. "Stromungserscheinugen in rotierend rohren", *VDI Forsch. Arb. Geb. Ing. Wes.*, **322**, p 18 (1929).

8. Shchukin, V.K. "Hydraulic resistance of rotating tubes", *J. Engng. Phys.*, **12**, pp 418–422 (1967).

9. Nuttall, J.B. "Axial flow in a vortex", *Nature*, **172**, p 582 (1953).

10. Talbot, L. "Laminar swirling pipe flow", *J. of Applied Mechanics*, **21**, pp 1–7 (1954).

11. Binnie, A.M. "Experiments on the slow swirling flow of a viscous liquid through a tube", *Quarterly J. Of Mechanical And Applied Mathematics*, **10**, pp 276–290 (1957).

12. Deka, B.C. "Some effects of weak swirl on laminar pipe flow", *Proc. of Nat. Inst. of Sci. in India, Part A*, **29**, pp 251–270 (1962).

13. Lavan, Z., Nielsen, H. and Fejer, A.A. "Separation and flow reversal in swirling flows in circular ducts", *The Physics of Fluids*, **12**, pp 1747–1757 (1969).

14. White, A. "Flow of fluid in an axially rotating pipe", *Mech Engng. Sci.*, **6**, pp 47–52 (1964).

15. Cannon, J.N. and Kays, W.M. "Heat transfer to a fluid flowing inside a pipe rotating about its longitudinal axis", *ASME J. Heat Transfer*, **91**, pp 135–139 (1969).

16. Borisenko, A.I., Kostikov, O.N. and Chumacheni, V.I. "Experimental study of turbulent flow in a rotating channel", *J. Engng. Phys.*, **24**, pp 770–773 (1973).

17. Murakami, M. and Kikuyama, K. "Turbulent flow in axially rotating pipes", *J. Fluids Engng.*, **102**, pp 97–101 (1980).

18. Kikuyama, K., Murakami, M. and Nishibori, K. "Development of three-dimensional turbulent boundary layer in an axially rotating pipe", *J. Fluids Engng.*, **105**, pp 154–160 (1983).

19. Kikuyama, K., Murakami, M., Nishibori, K. and Maeda, K. "Flow in an axially rotating pipe", *Bull. JSME.*, **26**, pp 506–513 (1983).

20. Nishibori, K., Kikuyama, K. and Murakami, M. "Laminarization of turbulent flow in the inlet region of an axially rotating pipe", *Bull. JSME*, **30**, pp 255–260 (1987).

21. Anwer, M. and So, R.M.C. "Rotation effects on a fully-developed turbulent pipe flow", *Experiments in Fluids*, **8**, pp 33–40 (1989).

22. Gethin, D.T. and Johnson, A.R. "Numerical analysis of the developing fluid flow in a circular duct rotating steadily about a parallel axis", *Int. J. Numer. Methods Fluids*, **9**, pp 151–165 (1989).

23. Yoo, G.J., So, R.M.C. and Hwang, B.C "Calculation of developing turbulent flows in a rotating pipe", *ASME J. Turbomachinery*, **113**, pp 34–41 (1991).

24. Reich, G. and Beer, H. "Fluid flow and heat transfer in an axially rotating pipe-I. Effect of rotation on turbulent pipe flow–II. Effect of rotation on laminar pipe flow", *Int. J. Heat Mass Transfer*, **32**, pp 551–574 (1989).

25. Chen, C.J., Bravo, R.H., Haik, Y.S., and Sheikholeslami, Z.M. "Numerical flow visualization of two-dimensional viscous flow in complex internal geometries", presented at the ASME Winter Annual Meeting, Nov. 27-Dec. 2, 1988, Chicago, IL, ASME-FED, **74**, pp 1–9 (1988).

26. Litsek, P.A. and Bejan, A. "Convection in the cavity formed between two cylindrical rollers", *ASME J. Heat Transfer*, **112**, pp 625–631 (1990).

27. Litsek, P.A., Zhang, Z. and Bejan, A. "Convection in the cavity between two rollers: the effect of thermal boundary conditions", *ASME J. Heat Transfer*, **113**, pp 249–251 (1991).

28. Burmeister, L.C. *Convective Heat Transfer*, John Wiley & Sons Inc., New York, USA (1983).

29. *FLUENT Manual*, Version 2.9 Update, Creare Incorporated, Hanover, NH, USA.

30. Patankar, S.V., *Numerical Heat Transfer and Fluid Flow*, Hemisphere, New York (1980).

31. Choudhury, D., Ambrosi, M. and Sheikholeslami, M.Z. "Solution of multi-dimensional fluid flow and heat transfer problems using body-fitted coordinates", *Proc. 1988 Ntl. Heat Transfer Conf.*, ASME HTD-96, **3**, pp 365–370 (1988).

32. *PLOT 3D User's Manual*, Version 3.5 with Appendix on Version 3.6, NASA, Fluid Dynamics Division (1989).

33. White, F.M. *Viscous Fluid Flow*, 2nd Edn., McGraw-Hill, Inc., New York, USA (1991).

34. Wong, K. "Laminar flow and heat transfer in contrarotating-wall ducts", Master of science thesis, University of Kansas, Lawrence, KS, USA (1992).

35. Wong, K. and Burmeister, L. "Laminar flow and heat transfer in a duct with contrarotating wall sections", *Enhanced Heat Transfer*, Proc., 28th Nat. Heat Transfer Conf., ASME HTD, **202**, pp 25–32 (1992).